Electronic Supplementary Material (ESI) for New Journal of Chemistry.

Supporting information

In-situ aqueous phase hydrodeoxygenation of methyl palmitate on Ni-Co alloy embedded in mesoporous carbon hollow spheres catalysts

Shangzhen Feng, Hantao Zhou, Zhongze Wang, Sihao Shu, Xing Zhang and Jixiang Chen*

Table S1 ICP elemental analysis of Ni and Co content in the catalysts.

	Ni wt%	Co wt%
NiCo@MCHS fresh	27.8	30.6
Filtrates obtained after 1 h HDO reaction	0.1	0.1
NiCo@MCHS used 5 times	27.4	30.1

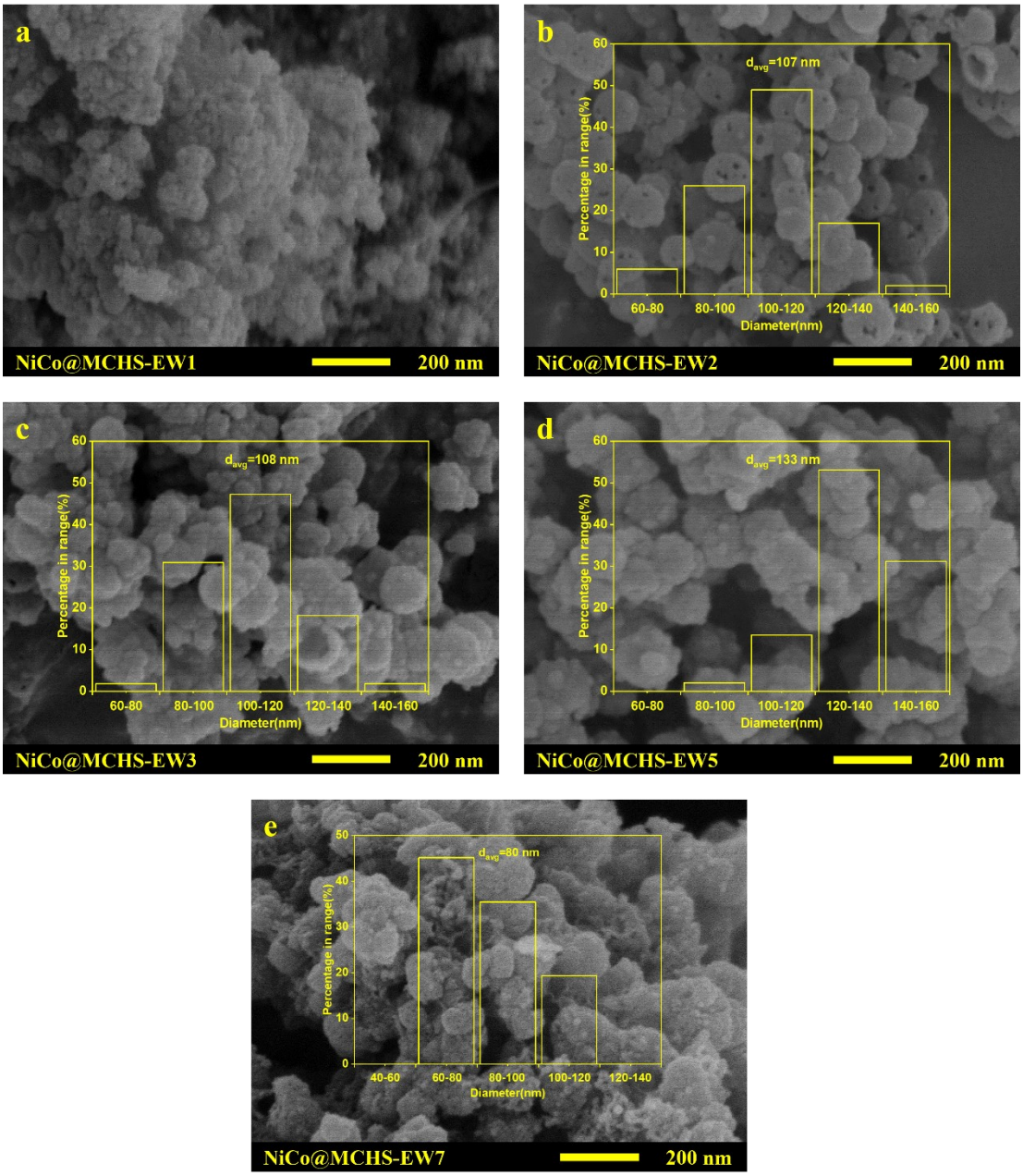

Fig. S1 SEM images of NiCo@MCHS with the ethanol/water volume ratios of (a) 1:1, (b) 2:1, (c) 3:1, (d) 5:1 and (e) 7:1.

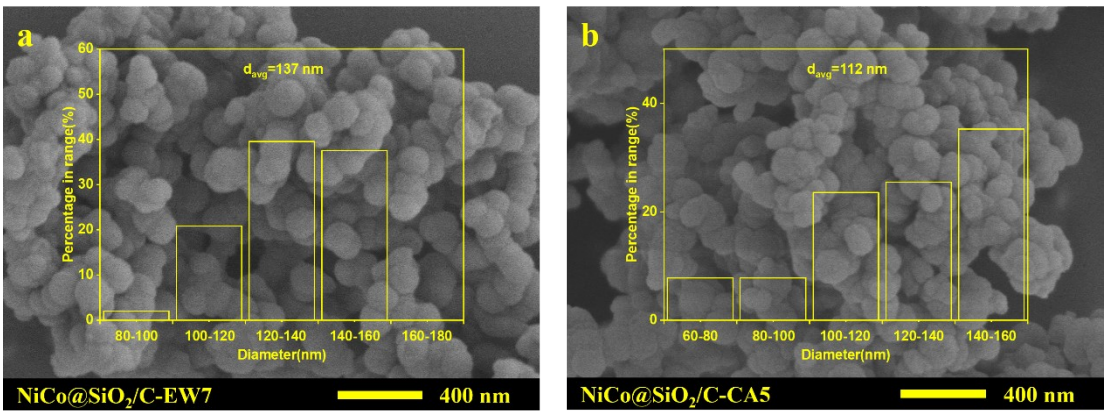

Fig. S2 SEM images of (a) NiCo@SiO_2/C-EW7 and (b) NiCo@SiO_2/C-CA5.

The SEM images of NiCo@MCHS prepared with different ethanol/water volume ratios are presented in Fig. S1. When the ethanol/water volume ratio is 1:1, excess water leads to rapid nucleation and growth of SiO_2 oligomers. Due to the size effect[1], the co-assembly of SiO_2 with RF is impeded. Consequently, catalysts are not spherical. As the ethanol/water volume ratio increases from 1:1 to 5:1, the spheres appear and their particle sizes increase from 107 to 133 nm, consistent with the findings reported by Liu et al.[2]. With increasing the ethanol/water volume ratio to 7:1, the hydrolysis of TEOS is sluggish. When the RF ceases to grow, free SiO_2 oligomers will continue to aggregate on the RF surface and subsequently grow. Consequently, NiCo@MCHS-EW7 exhibits average particle size of 80 nm, which is smaller than the 137 nm of NiCo@SiO_2/C-EW7 prior to etching (Fig. S1e vs. Fig. S2a).

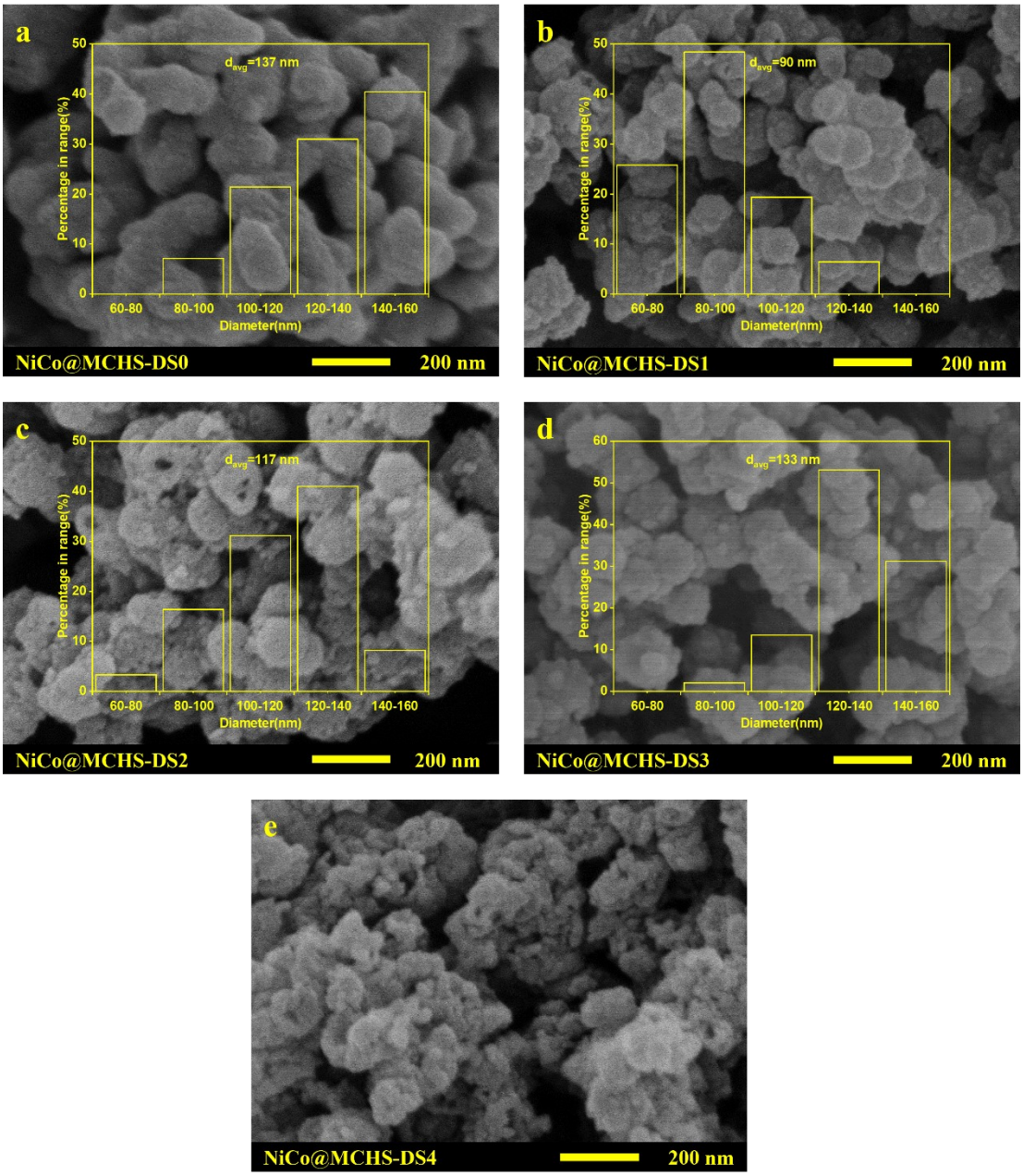

Fig. S3 SEM images of (a) NiCo@MCHS-DS0, (b) NiCo@MCHS-DS1, (c) NiCo@MCHS-DS2, (d) NiCo@MCHS-DS3 and (e) NiCo@MCHS-DS4.

The SEM images of NiCo@MCHS with different TEOS dosages are presented in Fig. S3. In the absence of template, the extensive cross-linking of RF results in non-uniform spheres with large particle size (137 nm). The addition of TEOS promotes the nucleation of RF by providing nucleation sites through the formation of SiO_2 oligomers, subsequently reducing the particle sizes. The average particle size of the catalyst increases from 90 to 133 nm as the TEOS dosage increases from 0.01 to 0.03 mol. Higher TEOS dosage results in more SiO_2 oligomers co-assembled with RF and larger SiO_2 cores. When the TEOS dosage is 0.04 mol, the morphology of the

catalyst is eliminated due to the excess SiO_2 oligomers.

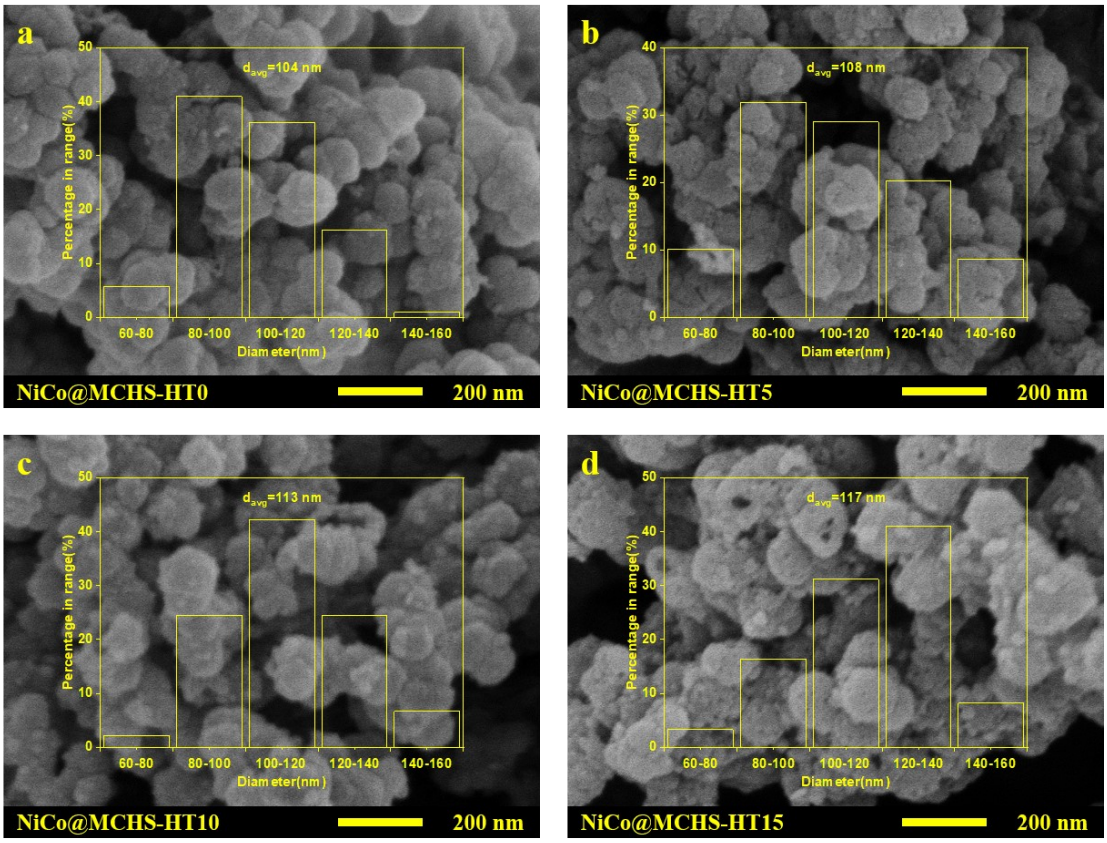

Fig. S4 SEM images of (a) NiCo@MCHS-HT0, (b) NiCo@MCHS- HT5, (c) NiCo@MCHS-HT10 and (d) NiCo@MCHS-HT15.

The SEM images of NiCo@MCHS prepared with different TEOS pre-hydrolysis time are shown in Fig. S4. Prolonged pre-hydrolysis time allows for the large SiO_2 cores and subsequently makes the catalyst particle sizes increase.

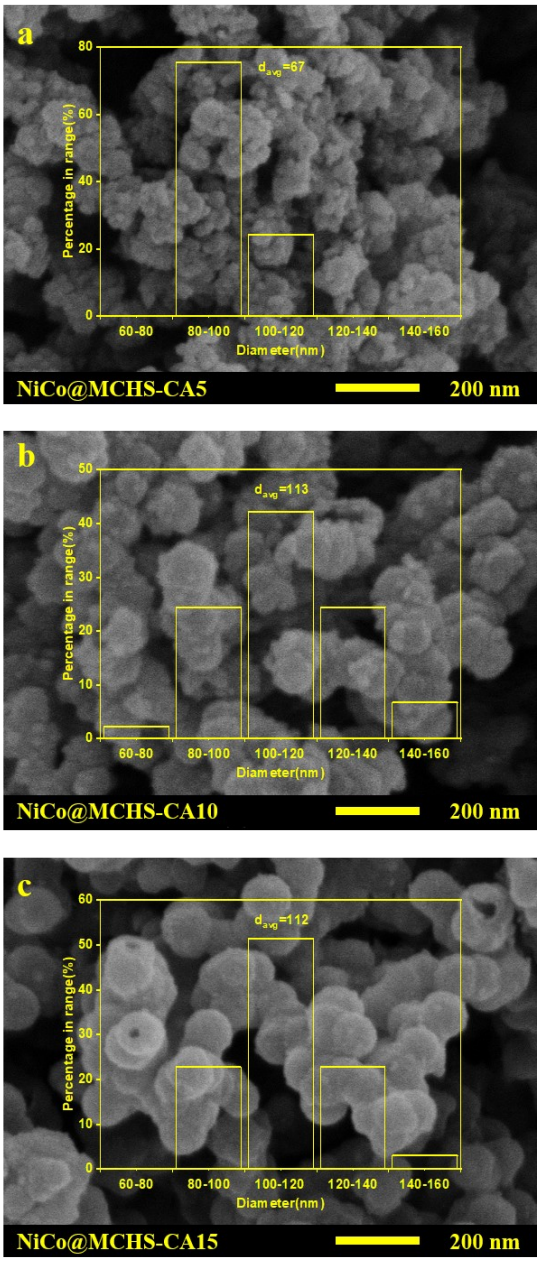

Fig. S5 SEM images of (a) NiCo@MCHS-CA5, (b) NiCo@MCHS- CA10 and (c) NiCo@MCHS-CA15.

The SEM images of NiCo@MCHS prepared with different dosages of ammonia solution are displayed in Fig. S5. The ammonia concentration affects TEOS hydrolysis, SiO_2 polymerization, RF polymerization[3], and the formation of metal hydroxides. Low ammonia solution dosage (5 mL) impedes the hydrolysis rate of TEOS for the formation of SiO_2 cores and growth during the pre-hydrolysis stage. As a result, a significant amount of SiO_2 oligomers aggregate on the RF surface, leading to a decrease in catalyst particle sizes from 112 to 67 nm after etching (Fig. S5a vs. Fig. S2b). And the catalyst morphology becomes irregular. In contrast, high ammonia

solution dosage (15 mL) facilitates the rapid formation of SiO_2 cores during the pre-hydrolysis stage, reducing availability of SiO_2 oligomers for mesopore formation.

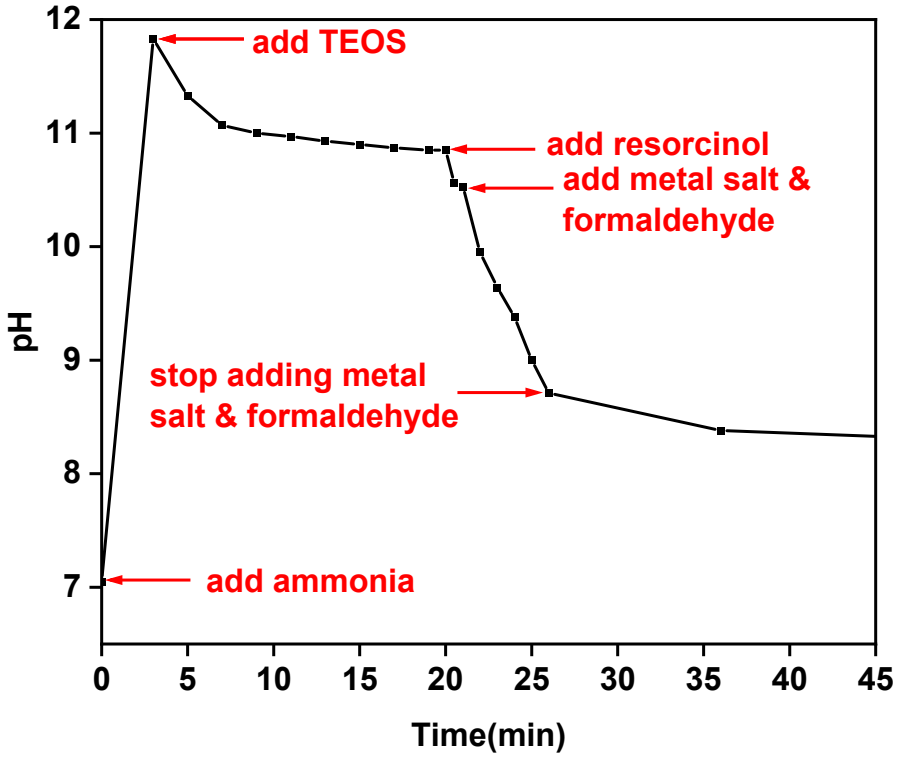

Fig. S6 Change of pH during NiCo@MCHS-DS2 preparation.

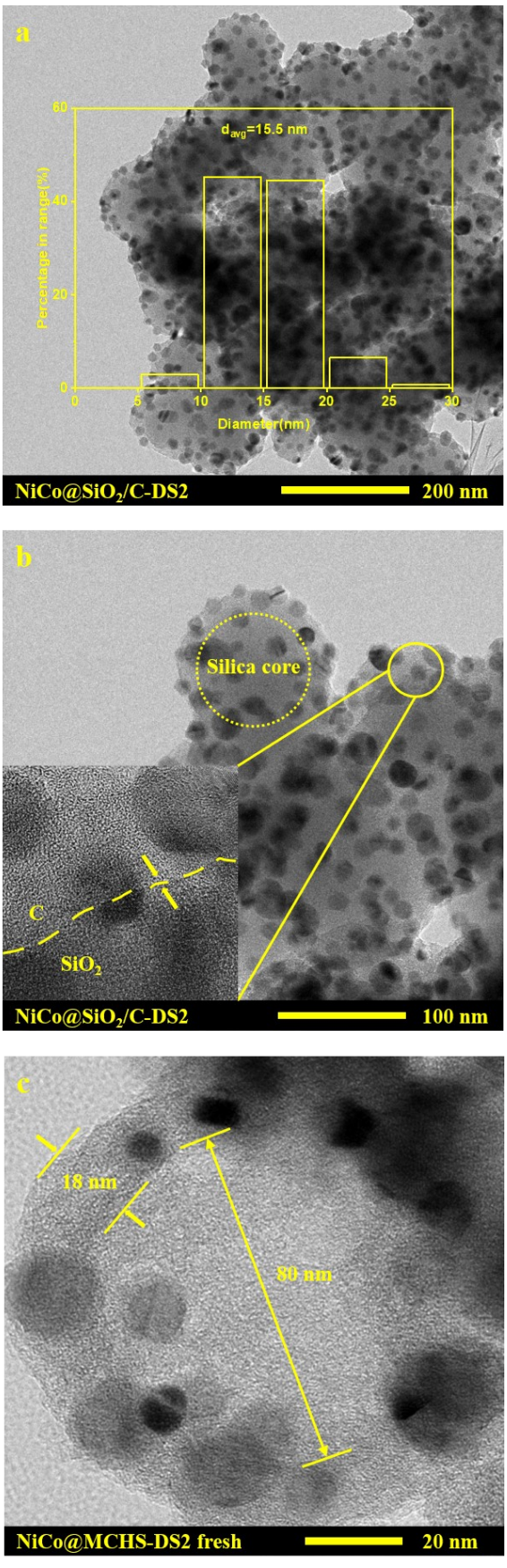

Fig. S7 TEM images of (a, b) NiCo@SiO_2/C-DS2 and (c) NiCo@MCHS-DS2.

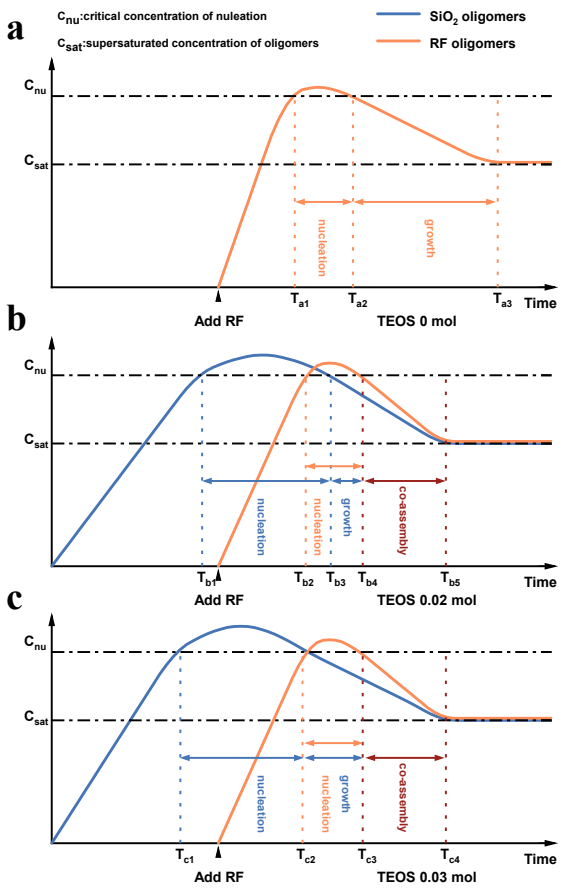

Fig. S8 Schematic representation of nucleation and growth of (a) NiCo@MCHS-DS0, (b) NiCo@MCHS-DS2 and (c) NiCo@MCHS-DS3.

Fig. S8 illustrates the nucleation-growth curves of SiO_2 and RF with varying dosages of TEOS. In the absence of TEOS (Fig. S8a), due to the lack of nucleation sites provided by SiO_2, RF undergoes a prolonged growth from T_{a2} to T_{a3}, ultimately forming large catalyst particle size. Upon the addition of 0.02 mol TEOS (Fig. S8b), SiO_2 grows up between T_{b3}~T_{b4}. This growth process extends to T_{c2}~T_{c3} at a TEOS dosage of 0.03 mol (Fig. S8c). Low TEOS dosage forms small SiO_2 cores, thereby yielding a diminished particle size for NiCo@MCHS-DS2 relative to NiCo@MCHS-DS3.

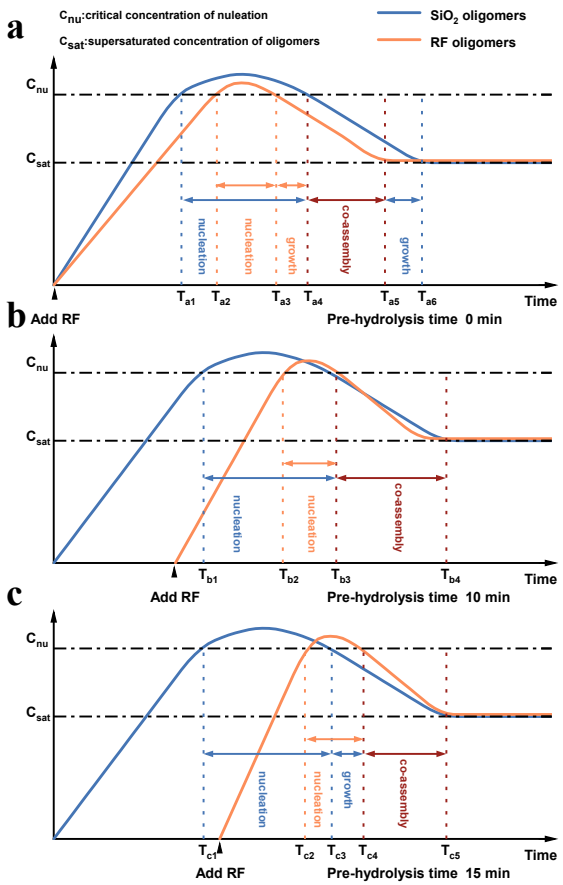

Fig. S9 Schematic representation of nucleation and growth of (a) NiCo@MCHS-HT0, (b) NiCo@MCHS-HT10 and (c) NiCo@MCHS-HT15.

The nucleation-growth curves of SiO_2 and RF at various pre-hydrolysis time of TEOS are depicted in Fig. S9. As the pre-hydrolysis time is prolonged, the concentration of SiO_2 oligomers increases at the moment of RF addition, consequently lengthening the growth time of SiO_2 cores and increasing the catalyst particle size.

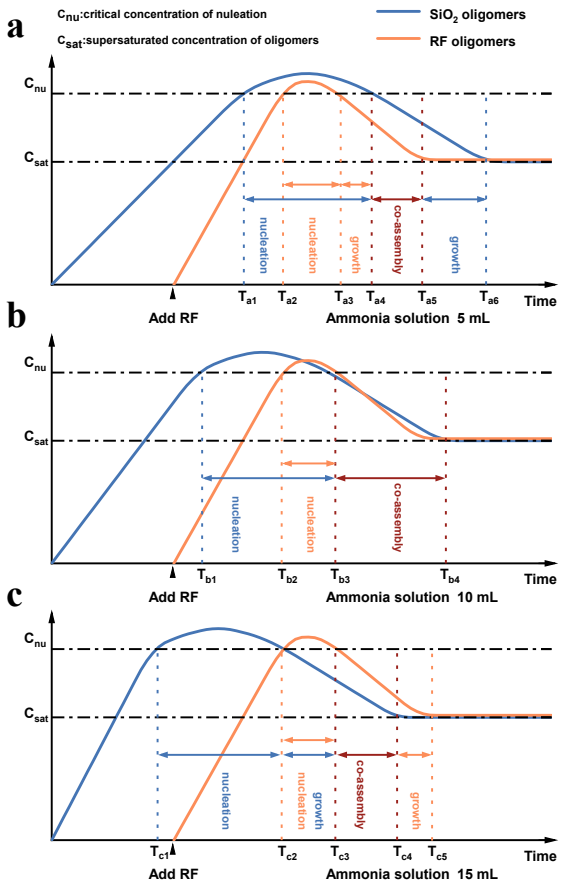

Fig. S10 Schematic representation of nucleation and growth of (a) NiCo@MCHS-CA5, (b) NiCo@MCHS-CA10 and (c) NiCo@MCHS-CA15.

Fig. S10 illustrates the nucleation growth curves of SiO_2 and RF with varying ammonia dosages. The hydrolysis rate of TEOS is low when the ammonia dosage is 5 mL (Fig. S10a). The nucleation-growth curve during this phase exhibits a resemblance to that of NiCo@MCHS-EW7 (Fig. 7c). With increasing the ammonia dosage to 15 mL (Fig. S10c), the hydrolysis rate of TEOS becomes too fast. The nucleation of SiO_2 oligomers between T_{c1}~T_{c2} and the growth of SiO_2 cores between T_{c2}~T_{c3} consume excess SiO_2 oligomers, resulting in a poor mesoporous structure (Table 2).

NiCo/MCHS catalyst was prepared via impregnation methods with MCHS as a support. In the synthesis process, 250 mL ethanol, 50 mL deionized water and 10 mL ammonia solution were firstly added into a flask followed by the stirring at 30 °C for 1 h, and then 0.02 mol of TEOS was added into the flask for pre-hydrolysis. After 15 min, 2 g resorcinol was added into the flask. When resorcinol was completely dissolved, the mixed solution (41.7 mL ethanol and 8.3 mL deionized water as solvent) of formalin was added dropwise into the flask. The mixture was stirred at 30 °C and 350 rpm for 24 h. After centrifugation, the polymers were washed with deionized water and ethanol three times and dried at 80 °C for 24 h to obtain the white SiO_2/RF composites. The SiO_2/RF precursors were carbonized on a fixed-bed quartz reactor under a N_2 flow (100 mL/min) according to the following temperature procedure: heated at a rate of 1 °C /min to 350 °C and holed for 3 h; heated at a rate of 2 °C /min to 800 °C and holed for 2 h. After the carbonization, the resulting samples naturally cooled to room temperature, which are denoted as SiO_2/C. Afterward, SiO_2/C was dispersed in 50 mL of 3 M NaOH solution, transferred to a 60 mL Teflon-sealed autoclave, and maintained at 80 °C for 24 h. After the subsequent centrifugation, washing and drying, the black MCHS powder was obtained. Then 2.13 g of $Ni(NO_3)_2 \cdot 6H_2O$ and 2.13 g of $Co(NO_3)_2 \cdot 6H_2O$ were impregnated on as-prepared MCHS support. The catalyst was obtained by reducing with 100 mL/min 10% H_2/N_2 flow on a fixed-bed quartz reactor at 400 °C for 1 h, and the final catalyst (denoted as NiCo/MCHS) was obtained.

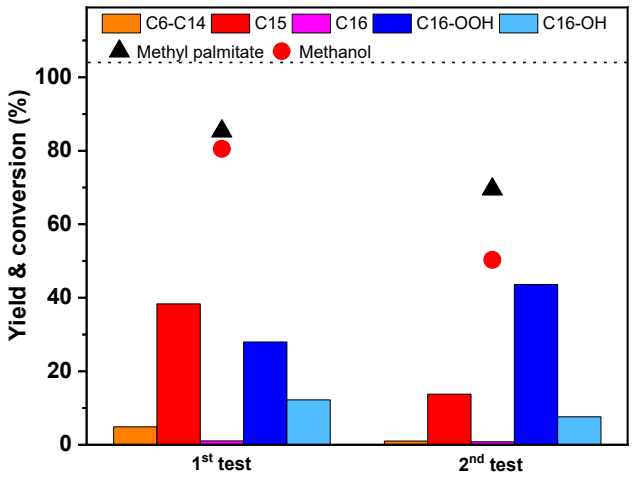

Fig. S11 Methanol and methyl palmitate conversions and products yields of NiCo/MCHS within in-situ HDO performance.

Reaction conditions: 310 °C, 4 g methyl palmitate, 3 g methanol, 8 g water, 0.4 g catalyst, 1 h.

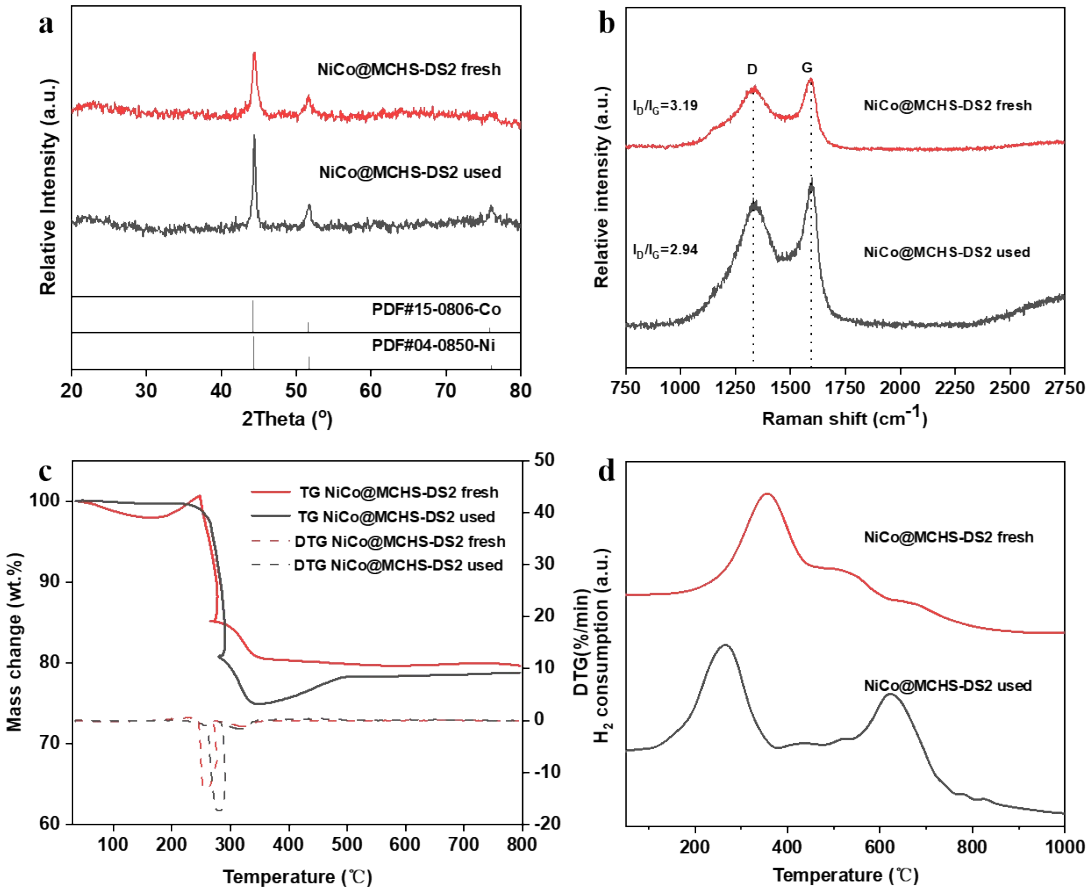

Fig. S12 (a) XRD patterns, (b) Raman spectra, (c) TG-DTG and (d) H_2-TPR curves of fresh and used NiCo@MCHS-DS2.

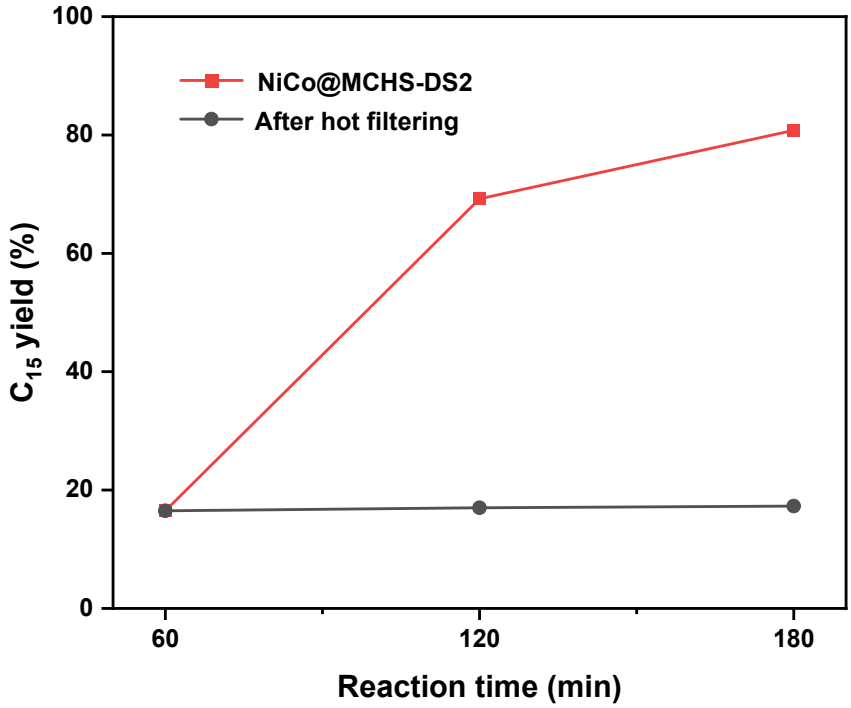

Fig. S13 Hot filtration experiment of NiCo@MCHS catalyst.

Reaction condition: 270 °C, 4 g methyl palmitate, 3 g methanol, 8 g water, 0.4 g catalyst.

References

1 N. H. Fletcher, J. Chem. Phys., 1958, **29**, 572–576.

2 J. Liu, S. Z. Qiao, H. Liu, J. Chen, A. Orpe, D. Zhao and G. Q. M. Lu, Angew. Chem. Int. Ed., 2011, **50**, 5947–5951.

3 L. Xie, M. Yan, T. Liu, K. Gong, X. Luo, B. Qiu, J. Zeng, Q. Liang, S. Zhou, Y. He, W. Zhang, Y. Jiang, Y. Yu, J. Tang, K. Liang, D. Zhao and B. Kong, J. Am. Chem. Soc., 2022, **144**, 1634–1646.